Astron. Astrophys. 297, 556–566 (1995)

ASTRONOMY AND ASTROPHYSICS

Fundamental parameters of galactic luminous OB stars

II. A spectroscopic analysis of HDE 226 868 and the mass of Cygnus X–1*

A. Herrero[1], R.P. Kudritzki[2,3], R. Gabler[2], J.M. Vilchez[1], and A. Gabler[2]

[1] Instituto de Astrofísica de Canarias, E-38200 La Laguna, Tenerife, Spain
[2] Universitäts-Sternwarte München, Scheinerstr. 1, D-81679 München, Germany
[3] Max-Planck Institut für Astrophysik, Karl-Schwarzschildstr. 1, D-85748 Garching bei München, Germany

Received 22 July 1994 / Accepted 8 October 1994

Abstract. We present a spectroscopic analysis of the O9.7 Iab star HDE 226 868, which is the optical counterpart of Cygnus X–1. We use this extreme supergiant to test the differences in the stellar parameters derived using plane parallel hydrostatic model atmospheres and spherical non–hydrostatic models ("Unified Model"). We find that the difference is significant, but smaller than it is needed to explain the mass and helium discrepancy between the theories of stellar atmospheres and evolution. We also find that the *dilution effect* of He I 4471 is not due only to the presence of a strong wind. We use the derived atmospheric parameters to show that Cygnus X–1 has to be a black hole (provided it is a single compact object) in a way that is independent of the distance to the system and assumptions about the mass–luminosity relation of the visible star. We also derive a probable mass for Cygnus X–1.

Key words: black hole physics – stars: atmospheres – stars: binaries: close – stars: fundamental parameters – stars: individual: HDE 226 868 – stars: individual: Cygnus X–1

1. Introduction

Cygnus X-1 is one of the most interesting objects in the sky. Since its detection as a strong X–ray source in the first days of X–ray astronomy (see Giacconi et al. 1967, and references therein; see also Tananbaum & Tucker 1974, for a review) has received a great deal of attention. After the detection of its rapid X–ray variability (Oda et al. 1971) and the identification of HDE 226 868 as its optical counterpart (Webster & Murdin 1972; Bolton 1972) it has been considered as one of the most firmly stablished black hole candidates.

HDE 226 868 was classified as an O9.7 Iab star by Walborn (1973) and the classification has been confirmed by Gies & Bolton (1986a). The spectroscopic parameters were determined by Conti (1978), who found values close to those we obtain here. Originally we included HDE 226 868 among the stars we observed in 1989, the analyses of which were published by Herrero et al. (1992, thereafter Paper I), but the analysis of HDE 226 868 proved to be more problematic than that of the other targets.

In our NLTE analysis of luminous galactic OB stars in Paper I we determined the stellar parameters of 25 such objects. From this study it became clear that there exists a discrepancy for many objects between the masses derived from the spectroscopic analysis and those predicted by the evolutionary calculations for single stars (e.g., those of Meader 1990) for the same temperatures and radii. We call this the mass discrepancy. The masses of the stars may be derived from the radiatively driven wind theory if V_∞ is known in addition to the stellar temperature and radius. The wind masses lie between the spectroscopic and the evolutionary masses, but are much closer to the former. On the other hand spectroscopic analysis also gives helium abundances that are above solar for a significant number of stars, a phenomenon not predicted by the evolutionary calculations. We call this the helium discrepancy. In both cases the discrepancy is larger for supergiants and is not significant for main sequence stars.

Both discrepancies might be of great importance for the theories of stellar atmospheres (photospheres and winds) and stellar evolution. To account for these discrepancies we have to introduce new physics into one or, more probably, both theories; for example, mixing processes in interiors (see Maeder 1987; Langer 1992; Denissenkov 1994) or sphericity and mass loss effects in atmospheres (see Gabler et al. 1989; Sellmeier et al. 1993; Schaerer & Schmutz 1994). In relation to this last point, it is clear that, because O stars show extended atmospheres and strong winds driven by radiation pressure, the plane parallel hydrostatic models used in Paper I could be inadequate for the analysis, especially in the case of supergiants.

Send offprint requests to: A. Herrero

* The INT is operated on the island of La Palma by the RGO in the Spanish Obervatorio de El Roque de los Muchachos of the Instituto de Astrofísica de Canarias.

HDE 226 868 was not included in the published analysis because its parameters, derived with the plane parallel hydrostatic model atmospheres used in Paper I led to contradiction with parameters derived from the published orbital data (see for example Gies & Bolton 1982). Thus, a more sophisticated analysis, incorporating the influence of sphericity and mass loss (*Unified Models*, see Gabler et al. 1989) seems unavoidable in this case. In addition, the star deserved especial attention because of its companion's nature.

The mass of the possible black hole has not been completely comfirmed until now. The reason is that all mass determinations of Cygnus X–1 rely on at least one of two unknown parameters, the distance of the system and the mass of the optical counterpart HDE 226 868 (see for example Gies & Bolton 1986a). The latter is usually estimated from its spectral type and luminosity class using spectral classification–stellar mass relations which rely on theoretical evolutionary models. This is problematic, first because of the discrepancies referred to above and secondly because, even if the evolutionary theory predicts correct masses for individual stars, the binary nature of the system could have given HDE 226 868 a mass–luminosity relation different from that of individual stars.

The spectroscopic analysis of HDE 226 868 with Unified Models allows us to adopt a new approach to the determination of the mass of Cygnus X–1 that is free from the two drawbacks mentioned above. Carrying it out we will determine the surface gravity and radius of the star, and thus its mass will be determined directly from the spectrum. The determination of the mass of the unseen companion will then follow, independently of the system's distance, and only assuming that it is a single compact object, as seems to be the case (Abt et al. 1977).

Of course, the star is not suitable for testing the discrepancies found in Paper I between the theories of stellar atmospheres and evolution of single stars, as the evolution in such a close system is probably very different from that of single stars. We will therefore not make a comparison with evolutionary tracks. But this is an adequate test of the influence of the mass loss and sphericity on the derived stellar parameters, which are also dealt with in the present paper.

In Sect. 2 we briefly describe the observations and in Sect. 3 we describe the spectrum. Section 4 presents the spectroscopic analysis made following the same method and using the same model atmospheres as in Paper I and in Sect. 5 we try to combine these results with the known orbital parameters and show that both sets of parameters are inconsistent. In Sect. 6 we present the results obtained using the Unified Models including sphericity and mass loss and in Sect. 7 we again combine the spectroscopic results with orbital data and then derive a minimum mass for Cygnus X–1. The probable mass is derived in Sect. 8. Section 9 is dedicated to a comparison of results from plane parallel and unified model atmospheres and to the corresponding discussion. Finally, the conclusions are presented in Sect. 10.

2. Observations and reduction of the spectra

The observations were carried out with the 2.5 m Isaac Newton Telescope at the Observatory of El Roque de los Muchachos in La Palma in 1989 July 17 and 18. The Intermediate Dispersion Spectrograph was used in two configurations: for the blue we used the H 2400 B grid with the 235 mm camera, which resulted in a spectral resolution of 0.6 Å FWHM measured on the Cu–Ar arc lines. For the red we used the 1800 V grid with the same camera, which resulted in a resolution of 0.8 Å FWHM.

The reduction of the spectra was performed as described in Paper I. We used the standard procedure of bias substraction, flat field division, spectrum extraction, wavelength calibration and continuum rectification.

3. Description of the spectrum

Figure 1 shows the optical spectrum of HDE 226 868 between 4 000 and 5 000 Å (approximately).

As has been said in the introduction, the star has been classified as O9.7 Iab by Walborn (1973). We have confirmed that the spectral characteristics are intermediate between those of HD 209 975 (19 Cep, O9.5 Ib) and HD 192 660 (B0 Ia) by comparing with our observations. We could not interpolate between the O9.7 Ia and Ib classes, but we confirm that the Si IV lines around 4100 Å are weaker in the O9.7 Ib star HD 18 409. The metal spectrum seems to be normal as compared with other supergiants of neighbouring spectral types (HD 227 634, HD 18 409, HD 209 975), again confirming Walborn's result.

We have used the metal lines to correct the different spectra for radial velocity. We excluded the strong hydrogen and helium lines, as they could be contaminated by wind emission and thus show an apparent displacement of the line centre. Then the individual spectra were merged to produce the spectrum of Fig. 1. The accuracy of the wavelength positions is about 0.3 Å or 20 km s^{-1}. The main source of uncertainty is the dispersion of results from the different metal lines used in the correction. The individual lines are allowed to vary inside this range when fitting the theoretical profiles.

After this correction we noted that the He II 4541 line seems to be redshifted by about 0.6 Å. No other line in the spectrum shows such a large displacement after the correction. Note that an apparent displacement to the red is just the opposite of what we should expect from wind contamination. If the line is contaminated by wind emission the red wing would be filled in and we would observe an apparent displacement to the blue. Although some physical (material moving away from us, blue shifted emission) or technical (problems with the spectrograph or the wavelength calibration in that zone) mechamisms could be invoked to explain it we do not have an explanation yet and will investigate the phenomenon in other analyses, comparing with similar data for other stars. For the present work, then, we will use the He II 4200 line. This line gives the same results as He II 4541 in this zone of the HR diagram (see Paper I).

Metal lines were also used for the determination of the projected rotational velocity. We obtained a value of 105 km s^{-1},

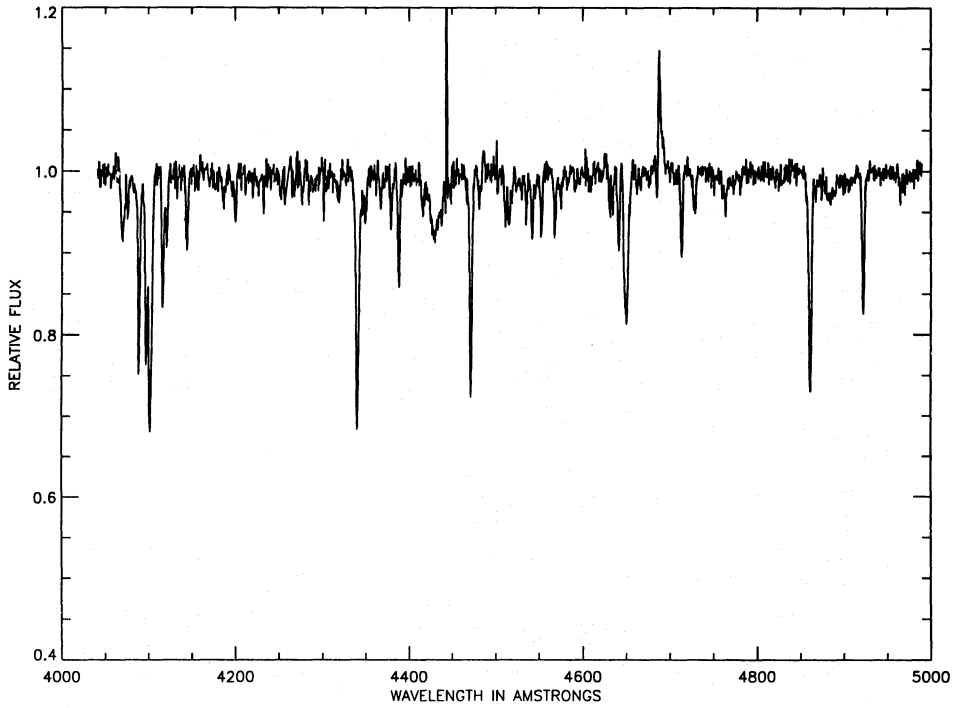

Fig. 1. The optical spectrum of HDE 226 868 from 4 000 to 5 000 Å. The emission at 4443 Å is a cosmic ray

which agrees with previous determinations (see Gies & Bolton 1986a)

4. Analysis with plane parallel models

We have performed two analyses, one with plane parallel models and one with Unified Model atmospheres (Gabler et al. 1989). As at present only a few studies using Unified Models exist, it is important to know the differences in the results obtained using both methods. Thus we begin by describing the analysis with plane parallel models.

The method followed to determine the stellar parameters from the spectrum using NLTE, plane parallel hydrostatic model atmospheres has been described in detail in Paper I and references therein. Briefly, we determine, at a fixed helium abundance, the gravity that best fits the different profiles of H and He at a given temperature, for a set of temperatures. If the abundance is right, the lines in the $T_{\rm eff}$–$\log g$ diagram will ideally cross at a point, giving the stellar $T_{\rm eff}$ and $\log g$. Usually, they form an intersection region, whose central point is taken as giving the stellar parameters, and whose limits give the adopted error. If the lines do not cross at any point, the helium abundance is changed. The helium abundance giving the smaller intersection region for all profiles is selected. The centre of the intersection region is taken again as the one giving the stellar parameters.

With this method we have determined the stellar parameters of HDE 226 868. We obtained $T_{\rm eff}$= 32 000 K, $\log g$= 3.0 (uncorrected for centrifugal force) and ϵ= 0.20 (abundance of helium with respect to the total abundance of hydrogen plus helium, by number. The solar abundance is ϵ= 0.09).

Having the stellar parameters as given above we can determine the radius, luminosity and mass of HDE 226 868 as described in Paper I (including the correction for the centrifugal force) by using the absolute magnitude given by Humphreys (1978). The needed values are listed in Table 2, together with the stellar parameters. Errors are again like in Paper I: $\pm$0.06 in $\log(R/R_\odot)$, $\pm$0.16 in $\log(L/L_\odot)$ and $\pm$0.22 in $\log(M/M_\odot)$.

5. The binary system: inconsistency with plane parallel model atmospheres

Usually we finish the analysis at this point. However on this occasion we are dealing with an interesting binary system and we could now derive the mass of the black hole candidate.

Let q be the ratio $M_{\rm O}/M_{\rm x}$, $M_{\rm O}$ and $M_{\rm x}$ being respectively the masses of the visible OB star and the companion, in solar masses. It may be determined from the known mass function (Gies & Bolton 1982). We have

$$f(M) = \frac{M_{\rm O}\sin^3 i}{q\,(1+q)^2} = 0.252 \pm 0.010\ M_\odot \qquad (1)$$

Thus having obtained $M_{\rm O}$ from the spectral analysis we need only the orbital inclination to derive the mass ratio q and the mass of the black hole candidate, $M_{\rm x}$.

From many determinations existing in the literature we find that the orbital inclination varies between 27° and 67° (see Ninkov et al. 1987 and references therein). Thus we can determine q as a function of the inclination angle for a given value of the mass and radius of HDE 226 868.

We have performed the calculation for the values given by the spectroscopic analysis and their extremes, the maximum and minimum values. To restrict the mass of the companion we

Table 1. Stellar parameters derived using plane parallel hydrostatic models (model A), Unified Models (model B) and Unified Models plus the assumption of aligned axes and orbital inclination of 35° (model C, final parameters). V is the stellar flux in the V band and M_v is the absolute visual magnitude taken from Humphreys (1978). Radius, luminosity and mass are given in solar units, $\dot{M}$ in solar masses per year and V_∞ in km s^{-1}. The gravities have been corrected for the effect of the centrifugal force

Model	$T_{\rm eff}$	log g	ϵ	V	M_v	$R/R_\odot$	log$(L/L_\odot)$	$M/M_\odot$	$-\log\dot{M}$	V_∞
A	32 000	3.03	0.20	-29.08	-6.3	22.9	5.7	20.4		
B	32 000	3.18	0.17			17.0	5.4	15.9	-5.52	2100
C	32 000	3.21	0.17			17.0	5.4	17.0	-5.52	2100

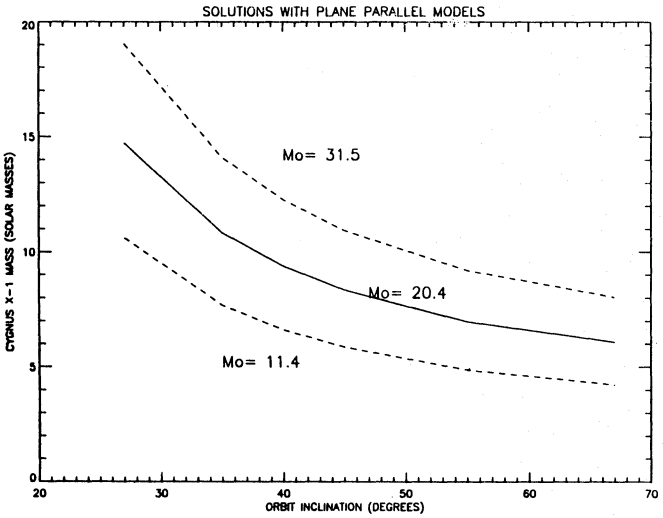

Fig. 2. The mass of Cygnus X–1 as a function of the orbital inclination for the HDE 226 868 mass deduced from the spectroscopic analysis with plane parallel models (solid line) and their extremes (the maximum and minimum values, dashed lines). The curves are labelled with the mass of the O star

use the upper and lower values of the mass function with the upper and lower values of the HDE 226 868 mass. To obtain the corresponding masses for Cygnus X–1 is then trivial, and we obtain the result plotted in Fig. 2. We see that the minimum mass we obtain for Cygnus X–1 corresponds to the minimum spectroscopic mass and the maximum orbital inclination, and has a value of 4.2 $M_\odot$, well above the masses determined for known neutron stars (Rappaport & Joss 1983) or the upper limiting mass for neutron stars models (see Chapter 9 of Shapiro & Teukolsky 1983).

At this point we could claim that we have found that the companion of HDE 226 868 has to be a black hole, assuming that it is a single compact object, and taking into account that a star of this mass should be visible (see Gies & Bolton 1986a). Unfortunately, our analysis is inconsistent, as it is shown by the determination of the Roche lobe radius. This can be determined from (see Paczynski 1974)

$$R_{\rm R} = A(0.38 + 0.2\ \log q), \qquad (2)$$

where $R_{\rm R}$ is the Roche lobe radius and A the separation of the gravity centres of HDE 226 686 and Cygnus X–1, in solar radii. A can be expressed as (see Pacyznski 1974)

$$A = a_1(1 + q), \qquad (3)$$

a_1 being the semi–major axis of the orbit of the O star (our notation here departs from that of Paczynski 1974). We actually know the corresponding projection, a_1 sin i, with i the orbital inclination. This projection is known to be 8.36 $R_\odot$ (see Gies & Bolton 1982).

If we now determine the radius of the Roche lobe for all possible values of the stellar mass and the orbital inclination we find that the stellar radius is always larger than the Roche lobe, and that the difference is larger than the errors. This is easily seen in Fig. 3, where we have plotted the Roche lobe radius against the stellar radius. The solid line defines the region allowed by the spectroscopic analysis. Above this line, the Roche lobe is larger than the stellar radius. Below it, the star overfills its Roche lobe catastrophically. The dashed lines show the region where the values of the Roche lobe radius are found from the orbital parameters combined with the parameters from the spectroscopic analysis. We see that there is no overlap, which means that both sets of parameters are incompatible.

The present analysis, however, relies on the value of M_v given by Humphreys and is actually equivalent to the assumption that the distance is known. In fact, if we allow that distance to vary, it is possible to find a solution at smaller spectroscopic radii. For values of the spectroscopic radius below 10 $R_\odot$ the Roche lobe is larger than the former one, and the data from the orbital and spectroscopic analysis would be compatible.

However, in this case the theory of radiatively driven winds (see Kudritzki et al. 1989) would predict terminal velocities of the order of 1000 km s^{-1}, far below the value given by Davis & Hartmann (1983) of 2300 $\pm$ 400 km s^{-1}. We regard this as a strong indication that this solution can be rejected.

Thus we have to conclude that the spectroscopic analysis is affected by the mass loss and the sphericity of HDE 226 868, which affect to the gravity and radius determinations.

We should point out that we did not consider here the effect of the inclination of the rotational axis or the contribution of turbulence to the line broadening, which could change the minimum mass slightly, but would have had no influence in the

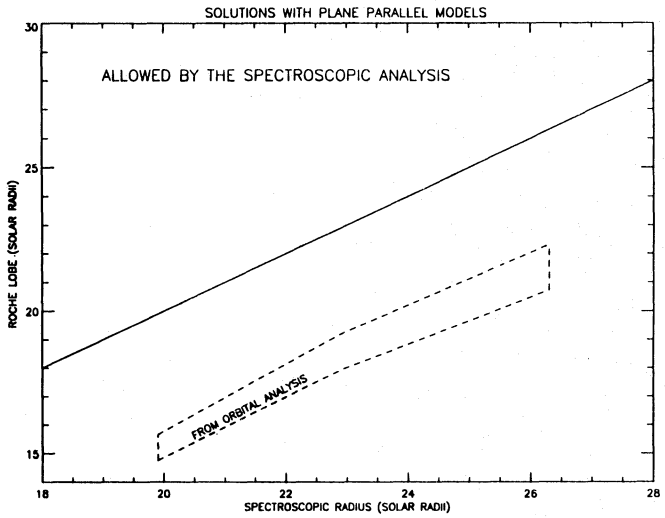

Fig. 3. Incompatibility of the parameters derived from the spectroscopic analysis using plane parallel models and the orbital parameters. The solid line is the 1:1 relation between the radius determined spectroscopically and the Roche volume radius. Above it, the Roche radius is larger. Below it, the spectroscopic radius is larger, meaning that the star would overfill its Roche lobe. All values of the Roche volume radius deduced from the analysis combining orbital and spectroscopic parameters are much lower than the corresponding stellar radius (region enclosed by the dashed lines)

conclusions. We will take these small effects into account in the following sections.

6. Analysis with unified models

The model atmospheres we use here have been described in Gabler et al. (1989). They are NLTE, spherical model atmospheres of H and He including mass loss. We call them Unified Models, because they do not separate photosphere and wind artificially.

The analysis of the observed spectrum is now complicated by the large number of variables in parameter space. Together with the temperature, gravity and helium abundance we must now specify the radius, mass loss rate and terminal velocity of the star (or some equivalent parameters).

Usually we start with the radius derived from the spectroscopic analysis. However on this occasion we know that this radius is unreliable. We also know that the star is a supergiant, a member of a close binary system, and that under this conditions it is quite probable that the star fills in its Roche lobe, as has been shown by Bolton (1975) and Gies & Bolton (1986b). We assume that this is the case, which allows us to be independent of M_v and thus of the distance for the radius determination. However, the Roche radius still depends on the stellar mass and the orbital inclination, which is unknown. For this reason we have started by choosing somewhat arbitrarily the Roche radius corresponding to the stellar mass deduced in the preceding paragraph (i.e. using plane parallel hydrostatic model atmospheres) for an inclination of 35°. This gives a radius of 19 $R_\odot$. Remember that this radius was incompatible with the mass and gravity derived from the plane parallel hydrostatic models.

We now have to fix the terminal wind velocity. We choose a velocity of 2100 km s^{-1}, which is typical for O9.7Iab stars (see for example the list of Howarth & Prinja 1989) and agrees with the value from Davis & Hartmann (1983). The influence of this parameter on the final emergent profiles is small, as long as we are dealing with photospheric profiles. For H_α the situation is more complicated, as its equivalent width is proportional to $\dot{M}^2 / (R^3 V_\infty^2)$ (Leitherer 1988). However the variations in V_∞ among O stars are much lower than the range of variation in $\dot{M}$. Thus the final effect of the unknown V_∞ on our results is mainly to increase the uncertainty due to $\dot{M}$ (see below).

To determine the mass loss rate we use H_α. Figure 4 shows the variation of the H_α profile for three values of the mass loss rate (0.51, 1.6 and 5.8 10^{-6} $M_\odot yr^{-1}$), obtained by keeping all other model parameters fixed. As we see, the profile changes dramatically. On the contrary, we see that the profile changes much less when we vary $\log g$ in 0.15 (Fig. 5). One can argue that a change of 0.15 in $\log g$ is not so much for the stellar parameters, but their consequences for the photospheric lines are as important as the dramatic changes in mass loss shown in Fig. 4. This is shown in Figs. 6 and 7, where we see the effect of the three values of the mass loss rate and the two different $\log g$ values on H_γ. From a comparison of both figures we see immediately that a change of 0.15 in $\log g$ has consequences in the wings that are comparable to those produced by a change of a factor 10 in the mass loss rate. From our experience with plane parallel hydrostatic models we know that a change of 0.15 in $\log g$ is comparable to a change of 2500 K in $T_{\rm eff}$. Thus, for a fixed pair ($T_{\rm eff}$, $\log g$) the changes in the mass loss rate will mainly affect H_α. Only when these changes are very large (say more than a factor 5) we will have to modify $T_{\rm eff}$ or $\log g$, or both, to fit the photospheric profiles again. This means that our results concerning the other stellar parameters (in particular gravity and mass) do not depend strongly on the fit of H_α.

At this point it is interesting to look at the He I 4471 profile. In Paper I we followed Voels et al. (1989) and studied the failure of the plane parallel hydrostatic models to correctly reproduce this line in supergiants, which led us to choose the weaker He I 4388 and He I 4922 lines for the analyses. According with the former authors we attributed this so-called *dilution effect* to the formation of the strong He I 4471 line in the upper layers of the photosphere, where the wind strongly influences its emergent profile. Thus, we would expect that the line becomes stronger in stars with stronger winds, i.e. with stronger mass loss rates. This is not the case, as can be seen in Fig. 8 where we show the He I 4471 line for the three models of Fig. 4. The change is small, and the minimum residual intensity is not reached for the model with the largest mass loss rate, but for the intermediate one. (Note also the apparent displacement to the blue of the calculated line in the case of strong mass loss). Thus we have to look for other explanations of the dilution effect. One possibility is the atomic model, where the treatment of the upper levels of the triplet system could be poor in stars of low

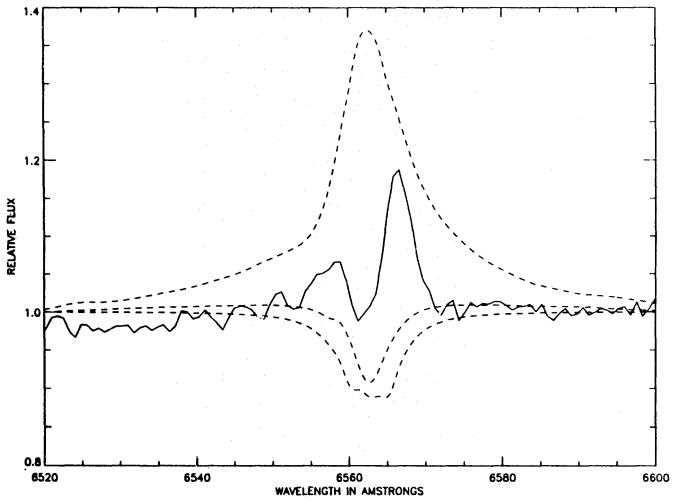

Fig. 4. Variations of the H_α profile with the mass loss rate. Full line: Observed profile in HDE 226 868; Dashed: calculated profiles with $\dot{M}$= 0.51, 1.6 and 5.8 10^{-6} $M_\odot yr^{-1}$. The models used had $T_{\rm eff}$= 30 000 K, log g= 3.15, ϵ= 0.17, $R/R_\odot$= 20.1, $M/M_\odot$= 20.7, V_∞= 2100 km s^{-1}

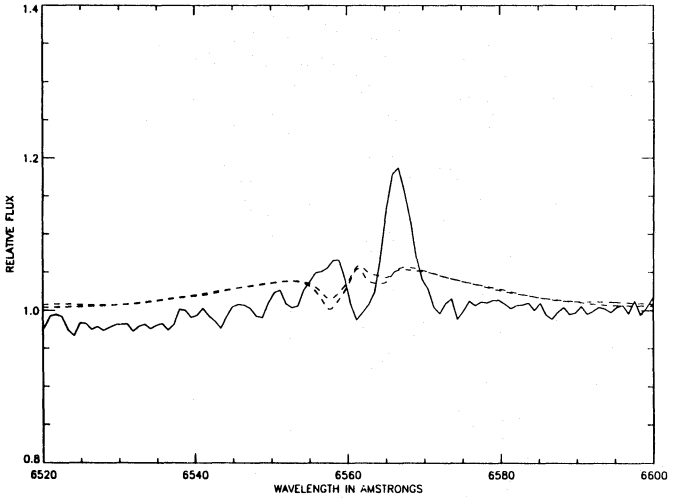

Fig. 5. Variations of the H_α profile with the gravity. Full line: Observed profile in HDE 226 868; Dash–dotted: calculated profiles with log g= 3.10, 3.25. The models used had $T_{\rm eff}$= 33 000 K, ϵ= 0.20, $R/R_\odot$= 19.6, $M/M_\odot$= 24.8, V_∞= 2100 km s^{-1} and log $\dot{M}$= 4.0 $10^{-6} M_\odot yr^{-1}$

gravities. This again shows that detailed calculations are always needed to test the explanations based on qualitative arguments.

From Fig. 4 we see already that the mass loss rate of HDE 226 868 will lie between 2 and 6 10^{-6} $M_\odot yr^{-1}$. However, we are not able to fit the detailed form of H_α with the Unified Models. This is not unusual, since we know that there is some contribution from the focussed wind, i.e. some contribution to the line emission from the inner Lagrangian point where the wind is dense, as has been shown by Gies & Bolton (1986b) using the model of Friend & Castor (1982).

Then we have first to decide which profile we will fit. We performed some test calculations with the Unified Models and saw that we can produce an absorption profile, a profile with a

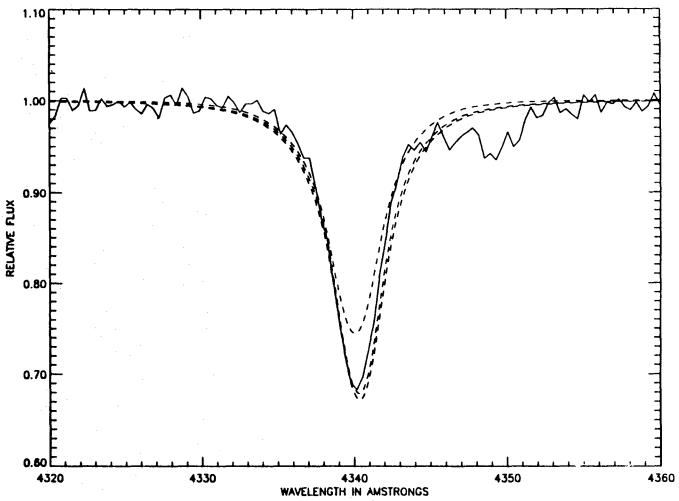

Fig. 6. Variations of the H_γ profile with the mass loss rate. Explanation as in Fig. 4

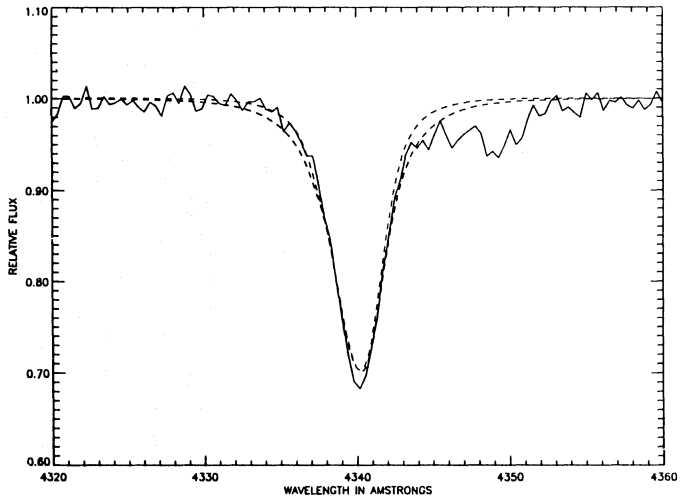

Fig. 7. Variations of the H_γ profile with log g. Explanation as in Fig. 5

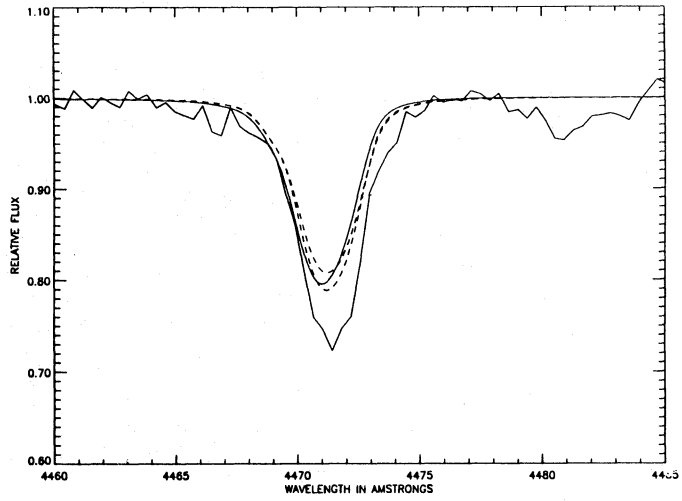

Fig. 8. Variations of the He I 4471 profile with the mass loss rate. Explanation as in Fig. 4, except that now the model with the upper mass loss rate has been plotted with a solid line for easier identification

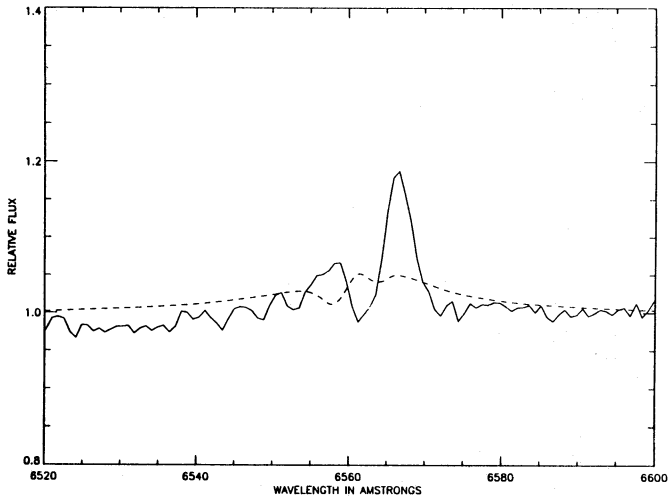

Fig. 9. Fit of the H_α line with the Unified Models

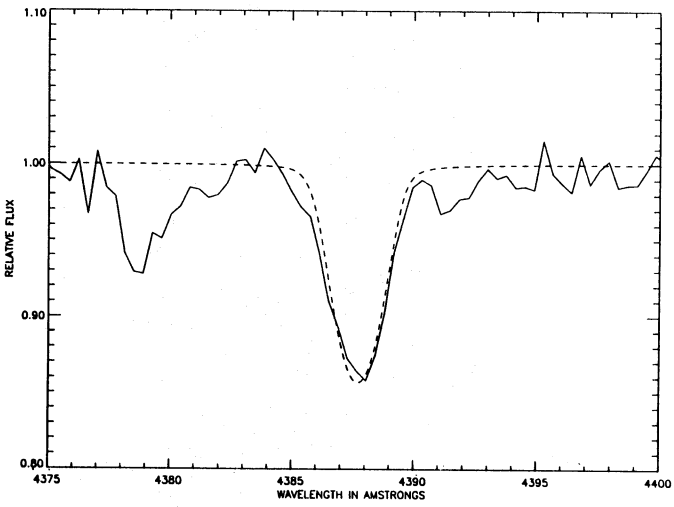

Fig. 11. Fit of the He I 4388 line with the Unified Models

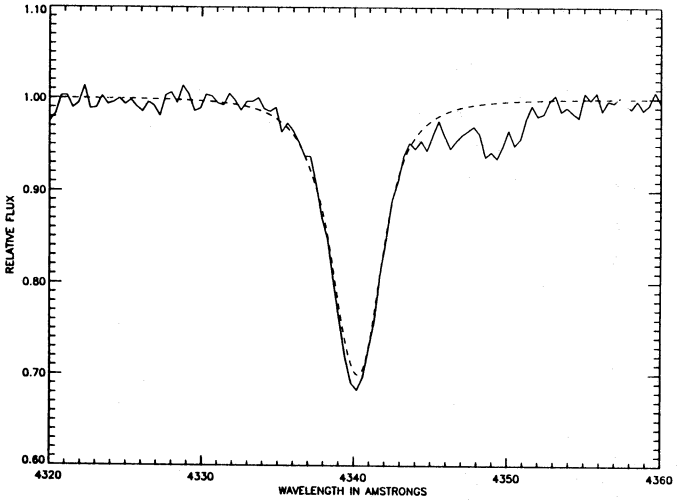

Fig. 10. Fit of the H_γ line with the Unified Models

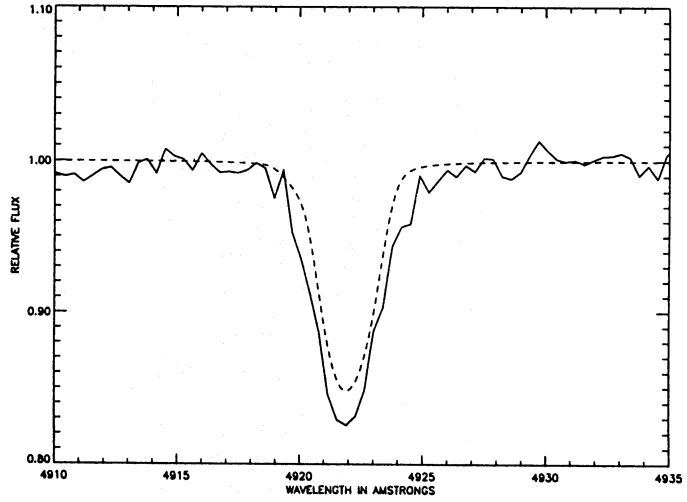

Fig. 12. Fit of the He I 4922 line with the Unified Models

double peak structure (increasing the mass loss rate) or a profile with a single broad emission peak nearly symmetric around the H_α central wavelength (increasing the mass loss rate even further). At first sight one would choose the mass loss rate giving the double–peak structure, but the calculated structure does not coincide with the observed ones: the positions of the peaks are different. Furthermore, at the position of the calculated peaks we do not see emission, which should be visible, because we assume that additional emission (not absorption) is present. Thus we choose the highest mass loss rate for which we do not see emission peaks in the calculated profile.

The uncertainty in the mass loss rate due to this effect (and to the unknown V_∞, see above) is not as large as might be thought, because the H_α profile is highly dependent on the assumed mass loss rate. We estimate the uncertainty in the derived mass loss to be less than a factor of 3 (see Fig. 5). Thus the photospheric profiles will be not significantly affected by this uncertainty.

Once we have fixed the radius and the mass loss rate we can fit the photospheric lines varying $T_{\rm eff}$, $\log g$ and ϵ as in Paper I. As the radius was arbitrarily chosen we have calculated several models changing the radius and repeating the procedure described above. We find that only $\log g$ has to be slightly corrected (increasing with decreasing radius).

Figures 9–16 show the fit obtained using Unified Models. The final parameters, given in Table I, are $T_{\rm eff}$= 32 000 K, $\log g$ (uncorrected)= 3.15, ϵ= 0.17, $R/R_\odot$= 17.0, $\dot{M}$ = 3.0 10^{-6} $M_\odot {\rm yr}^{-1}$, V_∞= 2100 km s^{-1}. We do not give errors for the derived stellar parameters, as we do not yet have a grid of theoretical models sufficiently narrow to set errors in the same form as we did with the plane parallel models. The corresponding luminosity and mass are $\log(L/L_\odot)$= 5.4 and $M/M_\odot$= 14.8. As in the plane parallel case, we have to correct for the centrifugal force. For $V_{\rm r}$= 105 km s^{-1} the correction to $\log g$ is +0.03. The mass would increase to 15.9 $M_\odot$.

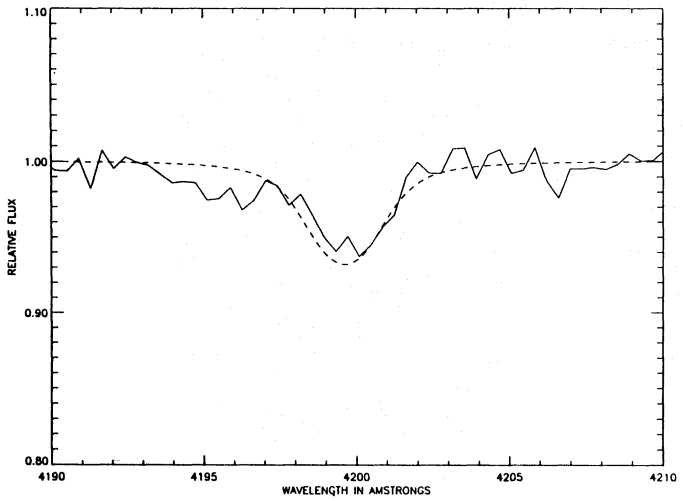

Fig. 13. Fit of the He II 4200 line with the Unified Models

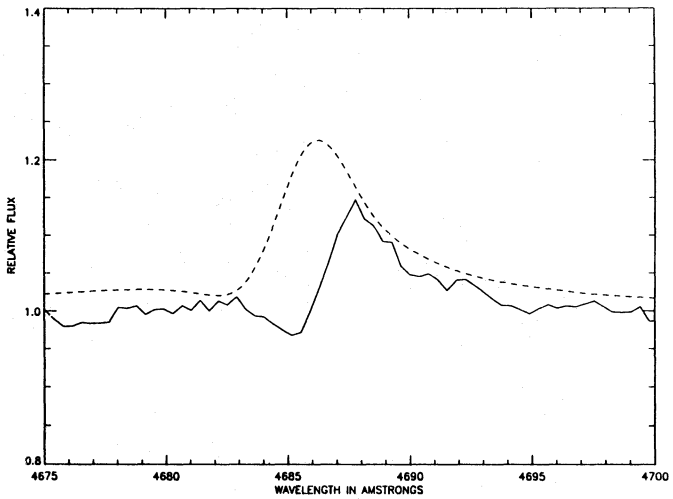

Fig. 16. Fit of the He II 4686 line with the Unified Models

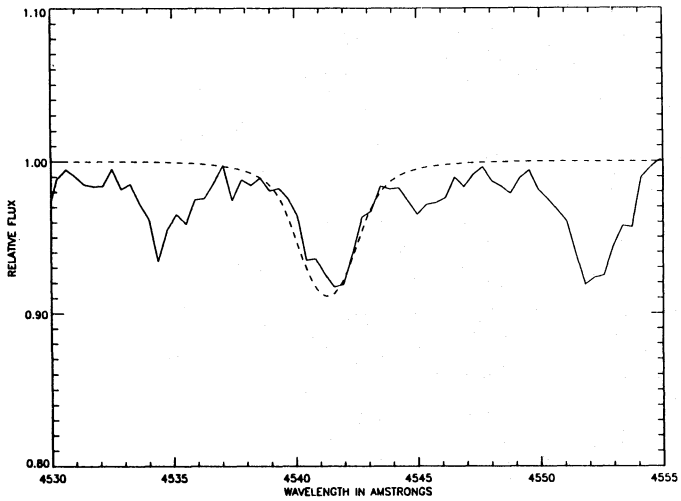

Fig. 14. Fit of the He II 4541 line with the Unified Models. The observed line has been displaced 0.6 Å to the blue

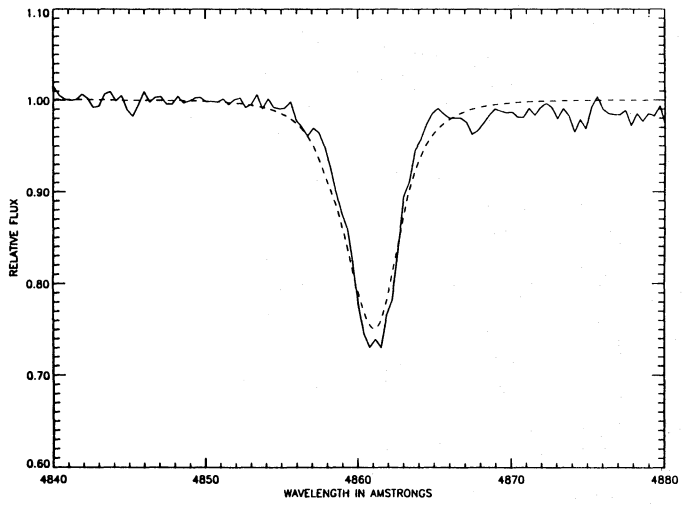

Fig. 15. Fit of the H_β line with the Unified Models

The calculated profile of the He I 4922 line is slightly too shallow, whereas that of He I 4388 is correct. This small discrepancy between the two lines was also noted in Paper I, where it was already indicated that the discrepancy corresponds to an uncertainty in $T_{\rm eff}$ of less than 1000 K, which is within the formal error box of the models.

Two more comments have to be made concerning the spectroscopic analysis. First, we can see that the calculated He II 4541 line reproduces the observed one well, except for the anomalous displacement. This could indicate that the origin of the displacement is artificial. Secondly, we see that the fit of the H_β and He II 4686 lines are very poor. None of the calculated H_β or He II 4686 profiles approaches the observed ones. For H_β this is striking, although it could be due to additional emission, as for H_α, but is not evident in the case of H_β. Increasing the mass loss rates up to levels significantly affecting the H_β line fit (as it is actually suggested by Fig. 15) would produce too much emission in H_α and H_γ. We still do not have an explanation for this behaviour of the H_β line and we are currently investigating whether it is a general problem of analysis with Unified Models or the particular case of HDE 226 868. In the case of He II 4686 we know that the lack of fit is a general problem of the Unified Models.

7. The binary system revisited

Having determined the atmospheric parameters of the O star in the preceding section including now sphericity and mass loss we can ask if we still have the same problems as with the parameters of the plane parallel models. Figure 17 displays the same kind of information as Fig. 3, i.e. the Roche volume radius derived for each value of the spectroscopic radius.

We see that now the situation is completely different. The solid line again divides the regions allowed and forbidden by the spectroscopic analysis, but now many possible solutions for the Roche radius fall in the allowed region. The maximum spectroscopic radius is now 17.5 $R_\odot$ because above it we are

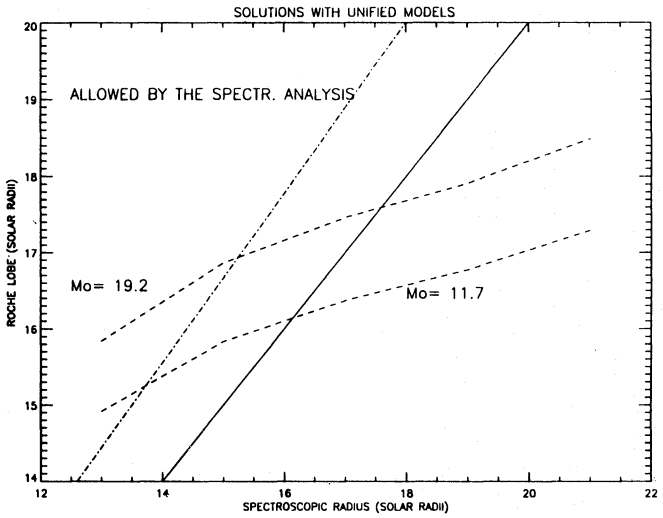

Fig. 17. The same as Fig. 3, now for Unified Models. The solid line divides the regions allowed (left) and forbidden (right) by the spectroscopic analysis. The dashed lines show the solutions at different orbital inclinations for the upper and lower limits of the mass of HDE 226 868. The dash–dotted line is the 1:0.9 relation, which Gies & Bolton (1986a) showed to be a lower limit

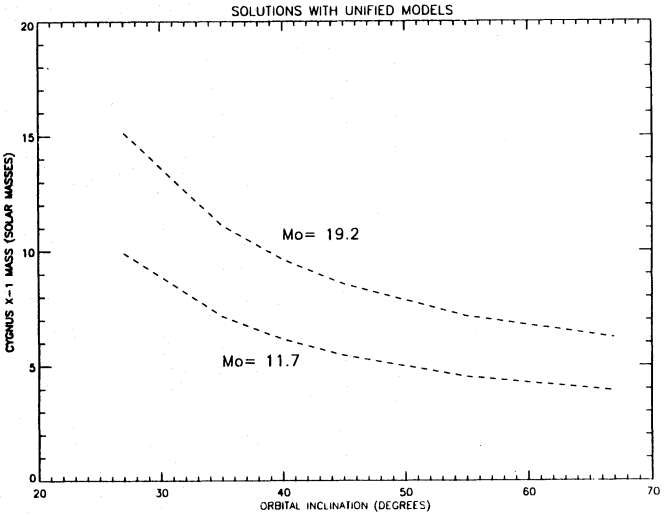

Fig. 18. Solution for the mass of Cygnus X–1 as a function of the orbital inclination for the upper and lower limit masses of HDE 226 868

in the region of forbidden solutions. 13.5 $R_\odot$is the minimum following the results of Gies & Bolton (1986a) who determined that the spectroscopic radius cannot be smaller than 90% of the Roche radius (dot–dashed line in Fig. 17). Thus the region of allowed solutions is now limited to the box enclosed by the four lines in Fig. 17. In addition, the solutions in that box are not only compatible with the optical spectrum, but also with the terminal velocity measured from the UV spectrum.

We can now set a lower limit to the mass of the companion of HDE 226 868. Figure 18 shows the possible masses for the extreme values of the spectroscopic mass (corresponding to the extreme values of the spectoscopic radius) as a function of the orbital inclination. Again, we use for the lower radius the lower value of the mass function and the lower value of $\log g$, and the corresponding upper values for the upper values of the spectroscopic radius.

As in the plane parallel case, we see that the minimum mass for Cygnus X–1 corresponds to the minimum spectroscopic radius of HDE 226 868 and the maximum orbital inclination. The value we obtain is 3.9 $M_\odot$, again above the upper limit for neutron stars. This limit could be lowered if we consider that part of the line broadening is due to some kind of turbulence, and not to rotation. This would decrease the correction to $\log g$ due to centrifugal force and would result in a smaller spectroscopic mass. Adopting a turbulence of 30 km s^{-1} (Gies & Bolton 1986a) results in a new lower limit of 3.8 $M_\odot$, which does not change anything.

Thus our analysis shows, *independently of the distance to Cygnus X–1 and the mass–luminosity relation of HDE 226 868*, that the companion of this star has to be a black hole, provided it is a single object (as is probably the case, see Abt et al. 1977).

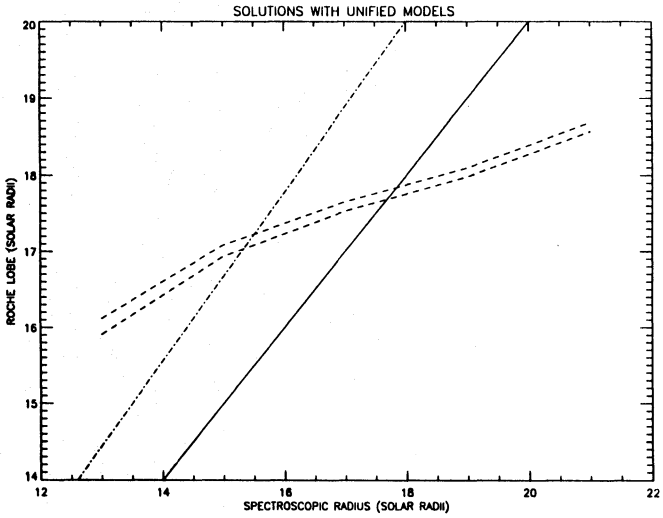

Fig. 19. Same as Fig. 17, but now for the orbital and rotational axes aligned, which implies a different correction to the centrifugal force for each inclination

8. The mass of Cygnus X–1

What is the probable mass of Cynus X–1 from our analysis? To answer this we will take advantage of the system's characteristics. We assume that HDE 226 868 rotates synchronously and with the rotational and orbital axes aligned. With these assumptions we can calculate the mass correction due to the centrifugal force for each inclination. This restricts the possible solutions in the (Roche radius—spectroscopic radius) plane as can be seen in Fig. 19. The minimum and maximum spectroscopic radii are now 15 and 17.5 $R_\odot$ respectively. As a consequence, the possible masses for Cygnus X–1 now vary between 4.8 and 14.7 $M_\odot$, depending mainly on the orbital inclination and, to a less extent, on the mass of HDE 226 868.

Although the orbital inclination has not been completely determined, a value of 35° falls in the center of all determinations in the literature, except that of Davis & Hartmann (1983), who give the range $36° < i < 67°$. Thus, if we assume that the orbital and rotational axes are aligned, the inclination of the rotation axis is also 35°, which would mean that the rotational velocity is 185 km s^{-1}. However, we have to consider the possible contribution of turbulence in the atmosphere. We use the value of 30 km s^{-1} quoted by Gies & Bolton (1986a). With this last correction we finally adopt a rotational velocity of 155 km s^{-1} for HDE 226 868. Adopting now our best model (that with 17 $R_\odot$), we finally obtain a value of 17.8 $M_\odot$ for the mass of HDE 226 868 , and 10.1 $M_\odot$ for Cygnus X–1.

9. Discussion

We return here to the original purpose of our work: the comparison of the results obtained with plane parallel and Unified Models and their possible influence on the solution of the mass and helium discrepancies.

We begin with the differences that could affect the mass discrepancy. First, we see that $\log g$ has changed by 0.15 dex. This result was expected from earlier test calculations (see Gabler et al. 1989; Sellmeier et al. 1993) and it is about half the change needed to explain the discrepancy between the atmospheric and evolutionary models found in Paper I. Thus, even in this extreme case, mass loss and sphericity alone cannot explain the mass discrepancy.

The masses from the plane parallel and Unified Models, however, are comparable. The reason is the change in radius, from 22.9 to 17.0 $R_\odot$. This change is probably an effect of the particular case we are dealing with, as it has been brought about by the additional information we have about the binary system. Although we still have not performed other analyses of massive OB stars in the detail presented here, in the test calculations we have performed so far it has not been neccesary to change the radius to such an extent, so this cannot be seen as a general result when changing from plane parallel to Unified Models.

Thus, we conclude that the sphericity and mass loss included in the unified models are able to explain part of the mass discrepancy (up to the half) as was suspected from test calculations. However, this statement is conditional on confirmation in future work that the change in radius is significant only for HDE 226 868 and will not be needed in further analyses.

We also found a small change in the helium abundance, in the direction of reducing the helium discrepancy. This, however, is totally insufficient to explain it. In the discussion in Paper I we have already included only stars with $\epsilon \geq 0.15$. Even reducing systematically all helium abundances above solar in Paper I by 0.03 would not improve the situation. Thus we again have to conclude that mass loss and sphericity alone cannot explain the helium discrepancy.

Future attempts to solve the discrepancies should include the effects of line blanketing (cf. Schaerer & Schmutz 1994) and of non–coherent electron scattering (cf. Rybiki & Hummer 1994) in the Unified Models .

10. Conclusions

We have shown in the previous sections that the companion of HDE 226 868 has a minimum mass above the upper mass limit for neutron stars, with a probable mass of 10 $M_\odot$. It is therefore a black hole, provided that it is a single compact object. This result is the first which is independent of the distance of Cygnus X–1 and of the mass–luminosity relation of HDE 226 868.

We have analysed HDE 226 868 by using plane parallel hydrostatic model atmospheres and by using unified model atmospheres including sphericity and mass loss. The comparison of results indicates that the introduction of these effects into the theory of stellar atmospheres cannot, by itself, explain the mass and helium discrepancies found in Paper I, although the first could be significantly reduced. In the future, however, a detailed analysis of a few single massive stars showing the mass discrepancy will be needed to be sure about possible changes in the spectroscopic radius.

We have found three problems in the analysis with Unified Models that we are not able to explain at present. The first is an anomalous redshift of the He II 4541 line, that could be artificial. The second is the failure of the H_β fit, which may only be a particular problem of HDE 226 868. We are currently analysing other stars to see if they show these two effects. The third problem is the failure of the He II 4686 fit, which we know from test calculations is a general problem of the Unified Models caused by an insufficient treatment of line blocking at EUV wavelengths around the HeII resonance line, which affects the populations of the second and third levels of HeII.

Acknowledgements. We would like to thank Dr Keith Butler and Dr Dietmar Kunze for helpful discussions, suggestions and calculations. A. Herrero thanks the Alexander von Humboldt Stiftung for a fellowship, during which part of the work was done, and the Universitäts– Sternwarte in Munich for their hospitality. The work was also supported by the Acciones Integradas Hispano–alemanas, a joint programme of the Spanish Ministerio de Educación y Ciencia (MEC) and the German Deutsche Akademische Austausch Dienst (DAAD).

References

Abbott D.C., Hummer, D.G., 1985, ApJ 294, 286
Abt H.A., Hintzen P., Levy S.G., 1977, ApJ 213, 815
Bolton C.T., 1972, Nature 235, 271
Bolton C.T., 1975, ApJ 200, 269
Conti P.S., 1978, A&A 63, 225
Davis R., Hartmann L., 1983, ApJ 270, 671
Denissenkov P., 1994, Double–zone model with diffusive mixing and the mass and helium discrepancies in OB–stars. In: Vanbeveren D., van Rensbergen W., de Loore C. (eds.) Evolution of massive stars: a confrontation between theory and observation, Kluwer Ac. Pub., Dordrecht, p. 405
Friend D.B., Castor J.I., 1982, ApJ 261, 293
Gabler R., Gabler A., Kudritzki R.P., Puls J., Pauldrach A., 1989, A&A 226, 162
Giacconi R., Gorenstein P., Gursky H., Waters J.R., 1967, ApJL 148, L119
Gies D.R., Bolton C.T., 1982, ApJ 260, 240
Gies D.R., Bolton C.T., 1986a, ApJ 304, 371

Gies D.R., Bolton C.T., 1986b, ApJ 304, 389
Herrero A., Kudritzki R.P., Vilchez J.M., et al., 1992 (Paper I), A&A 261, 209
Howarth I.D., Prinja R.K., 1989, ApJS 69, 527
Humphreys R.M., 1978, ApJS 38, 309
Kudritzki R.P., Pauldrach A., Puls J., Abbott D.C., 1989, A&A 219, 205
Langer L., 1992, A&A 265, L17
Leitherer C., 1988, ApJ 326, 356
Long K.S., Chaman G.A., Novick R., 1980, ApJ 238, 710
Maeder A., 1987, A&A 178, 159
Maeder A., 1990, A&AS 84, 139
Ninkov Z., Walker G.A.H., Yang S., 1987, ApJ 321, 425
Oda M., Gorenstein P., Gursky H., et al., 1971, ApJL 166, L1
Paczynski B., 1974, A&A 34, 161
Pauldrach A.W.A., Kudritzki R.P., Puls J., Butler K., Hunsinger J., 1993, A&A 283, 525
Rappaport S.A., Joss P.C., 1983, X–ray pulsars in massive binary systems. In: Lewin W.H.G., E.P.J. van den Heuvel E.P.J. (eds.) Accretion driven stellar X–ray sources. Cambridge Univ. Press, Cambridge, p. 1
Rybiki G., Hummer D.G., 1994, A&A, in press
Rosendahl J.D., 1970, ApJ 159, 107
Schaerer D., Schmutz W., 1994, A&A, in press
Sellmeier F., Puls J., Kudritzki R.P., et al., 1993, A&A 273, 533
Shapiro S.L., Teukolsky S.A., 1983, Black holes, white dwarfs and neutron stars, John Wiley & Sons, New York, p. 257
Tananbaum H., Tucker W.H., 1974, Compact X–ray sources. In: Giacconi R., Gursky H. (eds.) X–ray Astronomy, Reidel Pub., Dordrecht, p. 207
Voels S.A., Bohannan B., Abbott D.C., Hummer D.G., 1989, ApJ 340, 1073
Walborn N.R., 1973, AJ 78, 10, 1067
Walborn N.R., 1976, ApJL 179, L123
Webster B.L., Murdin P., 1972, Nature 235, 37

This article was processed by the author using Springer-Verlag LaTeX A&A style file version 3.